Unraveling Reactivity Differences: Room Temperature Ring-Opening Metathesis Polymerization (ROMP) vs. Frontal ROMP

Jacob J. Lessard,*[a] Edgar B. Mejia,[b] Abbie J. Kim,[a] Zhang Zhang,[b] Mya G. Berkey,[a] Zina S. Medina-Barreto,[b] Randy H. Ewoldt,[c] Nancy R. Sottos,[b] and Jeffrey S. Moore*[a,b]

a. Beckman Institute for Advanced Science and Technology, Department of Chemistry, University of Illinois Urbana–Champaign, Urbana, Illinois 61801, United States of America.

b. Beckman Institute for Advanced Science and Technology, Department of Material Science and Engineering, University of Illinois Urbana–Champaign, Urbana, Illinois 61801, United States of America.

c. Beckman Institute for Advanced Science and Technology, Department of Mechanical Science and Engineering, University of Illinois Urbana–Champaign, Urbana, Illinois 61801, United States of America.

Supporting Information Placeholder

ABSTRACT: In this study, we explore the distinct reactivity patterns between frontal ring-opening metathesis polymerization (FROMP) and room temperature, solventless ring-opening metathesis polymerization (ROMP). Despite their shared mechanism, we find that FROMP is less sensitive to inhibitor concentration compared to room temperature ROMP. By increasing the initiator-to-monomer ratio for a fixed inhibitor:initiator quantity, we find reduction in the ROMP background reactivity at room temperature (i.e., increased resin pot-life). At elevated temperatures where inhibitor dissociation prevails, accelerated frontal polymerization rates are observed due to the concentrated presence of initiator. Surprisingly, the strategy of employing higher initiator loading enhances both pot-life and front speeds, leading to FROMP rates exceeding prior reported values by over 5 times. This counterintuitive behavior is attributed to an increase in the proximity of the inhibitor to the initiator within the bulk resin and whether the temperature favors coordination or dissociation of the inhibitor. A rapid method was developed for assessing resin pot-life and a straightforward model for active initiator behavior was established. Modified resin systems enabled direct ink writing of robust thermoset structures at much faster rates than previously possible.

Ring-opening metathesis polymerization (ROMP) is a versatile and robust technique for synthesis of polymers tailored to diverse applications.[1-5] Manipulation of monomer, inhibitor, and initiator concentrations and identities has enabled precise control over polymer microstructure, size, and architecture.[6-15] Existing literature predominantly emphasizes the significance of conducting ROMP under meticulously controlled, air-free conditions, mild reaction temperatures, and (semi-)dilute concentrations.[16-21] As we venture beyond these 'ideal' conditions to explore bulk reactions, elevated temperatures, and non-inert environments, the applicability of traditional ROMP principles becomes increasingly ambiguous. This study investigates the boundaries of ROMP reactivity in unconventional settings, challenging established norms, and sheds light on the nuances that govern ROMP under diverse and less explored conditions.

Frontal polymerization is a promising application of ROMP, relying on a self-sustaining, exothermic reaction front directly converting bulk monomer into a polymeric material.[22-27] Specifically, frontal ROMP (FROMP) relies on the opening of strained cyclic olefins to generate heat as the monomer is consumed creating a localized and propagating front with a temperature gradient from room temperature up to 250°C.[28-37] Unlike ROMP where initiation, propagation, and termination happen both sequentially and globally, the presence of the propagating front in FROMP has these steps activating locally. As the local reaction occurs, the heat generated diffuses to surrounding regions to again trigger initiation then propagation. The saturated conditio-

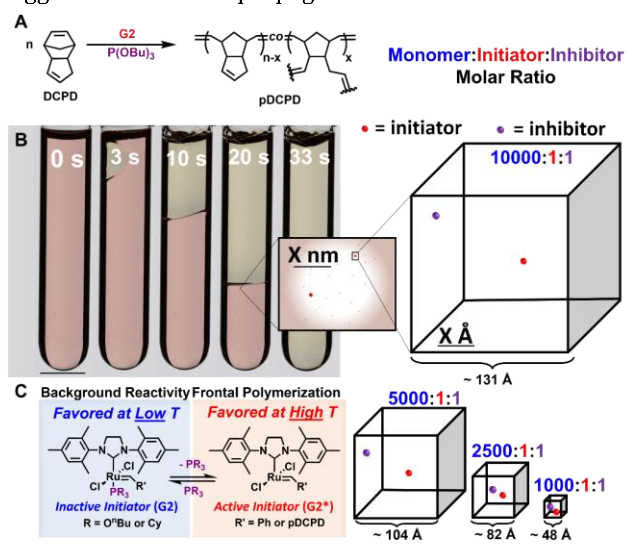

Figure 1: (A) Reaction scheme for frontal ring-opening metathesis polymerization (FROMP) of dicyclopentadiene (DCPD, monomer) using Grubbs' 2nd generation catalyst (initiator), and tributyl phosphite (TBP, inhibitor). (B) FROMP of DCPD resin (pink, 10,000:1:1 monomer:initiator:inhibitor, 0.01mol% initiator & inhibitor) to pDCPD thermoset (yellow, scale bar=10mm) from local heat activation. (C) Proposed inhibition

mechanism for FROMP and background ROMP with depiction of relative proximity for varying initiator loadings.

-ns, rapid local reaction rates, and large temperature variance of FROMP make direct correlation to solution-state ROMP unrealistic. To understand these polymerizations a top-down approach becomes necessary, evaluating front propagation rate, temperature profile, and resulting material properties. Additionally, reactivity of the bulk resin at lower temperatures (pot-life) gives insight to the trends between resin mixtures and the practical working window of the resin prior to gelation (viscoelastic liquid to solid transition). Ideally, FROMP resins possess long pot-life (low room temperature reactivity) but fast fronts (high temperature reactivity); intuitively, these reaction rates are coupled.[38]

In this work, we successfully decouple the rates of frontal polymerization and bulk ROMP, despite their shared reaction mechanism. Our objective is twofold: first, to decrease the background reactivity of the resin, and second, to significantly enhance the FROMP rate beyond the conventional ~1mm/s benchmark. To achieve this, we manipulate both initiator and inhibitor levels, thereby altering the effective initiator concentration at both room temperature and the elevated temperatures encountered during FROMP. Given the preference for inhibitor dissociation at higher temperatures, we hypothesize that FROMP will exhibit reduced sensitivity to inhibitor concentration compared to room temperature ROMP, as illustrated in Figure 1.[39] Additionally, we harness the controlled nature of ROMP to generate polymers with lower molecular weight at higher initiator loading. This deliberate choice limits polymer entanglement, thereby extending the pot-life of the resin.[40]

We began our study by examining FROMP resins under prior initiator loading conditions (10,000equiv monomer to initiator, 0.01mol% initiator) to establish a baseline for our subsequent initiator variation experiments.[41-45] By manipulating only the inhibitor loading relative to the initiator concentration, we observed a notable increase in the front velocity of FROMP (v_f), reaching 1.54±0.09mm/s at 0.25equiv inhibitor compared to 0.27±0.02mm/s at 8.00equiv inhibitor (Figures 2A, S1-13). This exploration revealed a clear correlation: reducing the inhibitor content led to a higher v_f. To gain deeper insights into the reactivity of these resins, we conducted room temperature studies using oscillatory shear rheology, analyzing parameters such as storage modulus (G', representing the elastic component) and loss modulus (G'', representing the viscous component). The crossover point at which G' equaled G'', provides an approximation of the resin's gelation time and pot-life—when the material transitions from a viscoelastic liquid to a viscoelastic solid. Our observations revealed a trade-off: the enhanced v_f came at the expense of increased resin background reactivity. Resins with faster fronts exhibited significantly accelerated background ROMP reactions (Figures 2B, S14-16). At 30°C, the crossover times were 2,500±600s, 6,100±800s, and 21,000±1,500s for 0.25, 1.00, and 4.00equiv inhibitor, respectively, highlighting the balance between front velocity and background reactivity in FROMP resins. Lastly, glass transition (T_g, glassy to rubbery transition temperature) of the polymer network remained relatively constant for loadings 2.00equiv or lower before a large drop in T_g for inhibitor loadings over 4.00equiv (Figures 2C, S17-22), further emphasizing the tradeoff of high inhibitor loadings.

In our pursuit of efficient and high-throughput testing methods for FROMP resins, we established a protorheology approach, designed for straightforward quantitative rheologic analysis (Figure 2D).[46] To assess the gel

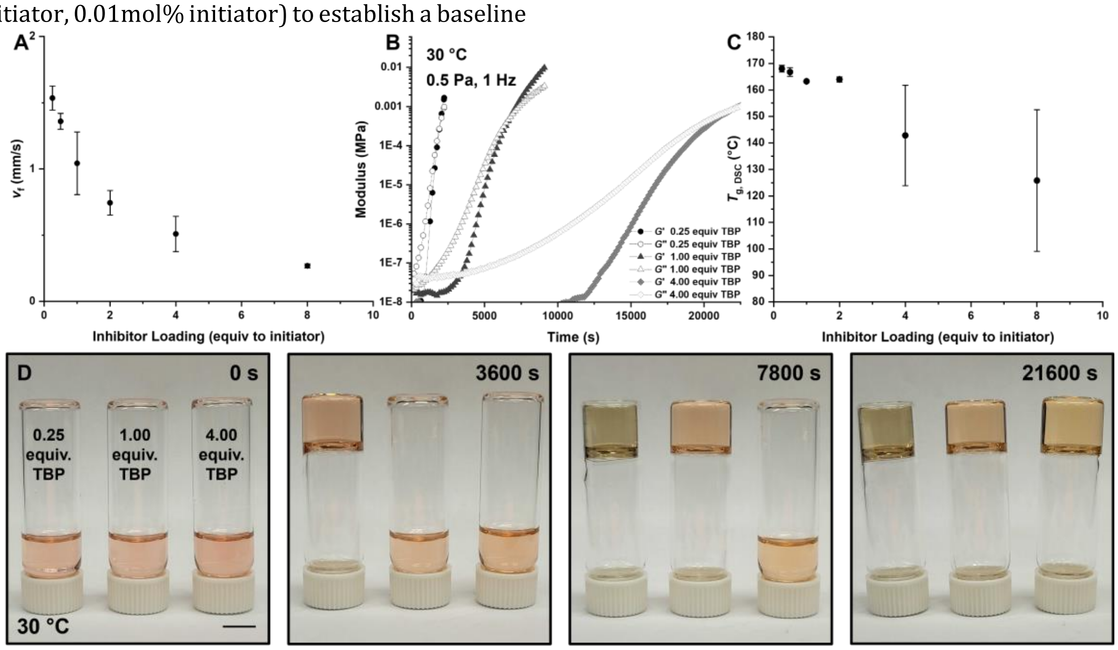

Figure 2: (A) Front velocity (v_f) of FROMP resins with varied loadings of inhibitor (10000:1:x monomer:initiator:inhibitor) showing a decrease in v_f with increasing inhibitor loading. (B) Shear rheology of FROMP resins at 0.25, 1.00, and 4.00equiv inhibitor showing an increase in resin lifetime (pot-life) at 30°C. (C) Glass transition temperatures (T_g) for the pDCPD after FROMP showing plasticization of networks at high inhibitor loadings (≥4.00equiv TBP). (D) Representative protorheology "inverted vial tests" for the evaluation of gelation at different t_{rest} at 0.25, 1.00, and 4.00equiv TBP (scale bar=10mm) agreeing well with observed viscoelastic crossover from shear rheology.

point of the resin network using protorheology, we employed an inverted vial test. This test entails heating the sample and, after a specific rest time (t_{rest}), inverting the vial to observe its ability to creep—deform under the influence of gravity—for an observation time (t_{obs}) of 10s. We hypothesized that no observable resin displacement after inversion (<1mm within t_{obs}) corresponds to a large increasing viscosity and an approximation of the gel point. We inferred gel times of 3,500±600s, 7,500±700s, and 21,600±100s, for 0.25, 1.00, and 4.00equiv inhibitor, respectively at a resting temperature of 30°C. These values closely align with the viscoelastic moduli crossover times obtained through shear rheology (Figure S23), validating the utility of protorheological data for rapidly estimating gel point.

In our quest to strike a balance between front rate, background reactivity, and material properties, the findings above suggest an optimal range of 1-2equiv of inhibitor at the 10,000:1:x monomer:initiator:inhibitor loadings. It may appear that further adjustments in initiator and inhibitor loadings could jeopardize either fast front speed or slow background reactivity. Moreover, the bulk nature of these resins means that altering the monomer to initiator ratio not only changes the inhibitor and initiator concentration but also impacts the inhibition equilibrium, the initial step in the polymerization mechanism, affecting both initiation and propagation processes.

We investigated the pivotal role of G2, where it transitions from the inhibitory state to the active initiator state (G2*, the coordinatively unsaturated 14-electron complex), a crucial step governed by the local proximity of the initiator and inhibitor (Figure 3A, Equations S1-2, Tables S1-3). Employing a simple equilibrium approximation, we observed a consistent increase in onset temperature with increasing inhibitor in the model profile, predicting the trends in the DSC thermograms (Figures 3B, S24-25). When the same model is applied to samples with heightened initiator and inhibitor loadings, the model revealed a static onset temperature but a proportional increase in [G2*] loadings at the elevated temperatures characteristic of FROMP (>200 °C). This static onset suggests a constant [G2*] across all samples at lower temperatures but a higher [G2*] (proportional to initiator loadings) at higher temperatures, resulting in similar background ROMP rates but more rapid FROMP rates at higher initiator loadings. This observation aligns well with the DSC cure kinetic profiles, highlighting the effectiveness of the model in capturing the intricate dynamics of the polymerization process (Figure 3C).

We hypothesized that low-temperature ROMP would exhibit similar behavior across all samples with equivalent initiator and inhibitor loadings (x:1:1 monomer:initiator:inhibitor), while significant differences in reaction rates would emerge at the elevated temperatures characteristic of FROMP. ROMP kinetics from (proto)rheology and molecular weight measurements conducted at 30°C (Figures 4A-B, S26-35, Tables S4-5) revealed that high initiator concentrations prolonged the resin lifetime, a phenomenon attributed to the lower molecular weight achieved at similar conversion rates. This extension in resin lifetime is attributed to the longer time required to attain the critical polymer entanglement molecular weight at the resulting polymer concentration (proportional to initial initiator loading),[47] a consequence of the living nature of ROMP. We proceeded to investigate frontal polymerization kinetics at varied loadings (Figures S36-65, Table S6-7), and observed a consistent increase in front velocity (v_f) with higher inhibitor loadings. Frontal polymerization rates were measured at 1.0±0.2mm/s, 1.5±0.4mm/s, 2.0±0.4mm/s, 2.5±0.2mm/s, and 3.7±0.2mm/s for 10,000:1:1, 5,000:1:1, 2,500:1:1, 1,000:1:1, and 500:1:1 loadings, respectively. Notably, the final materials exhibited minimal changes in T_g, affirming the integrity of the produced polymers under varying conditions (Figures S66-S73).

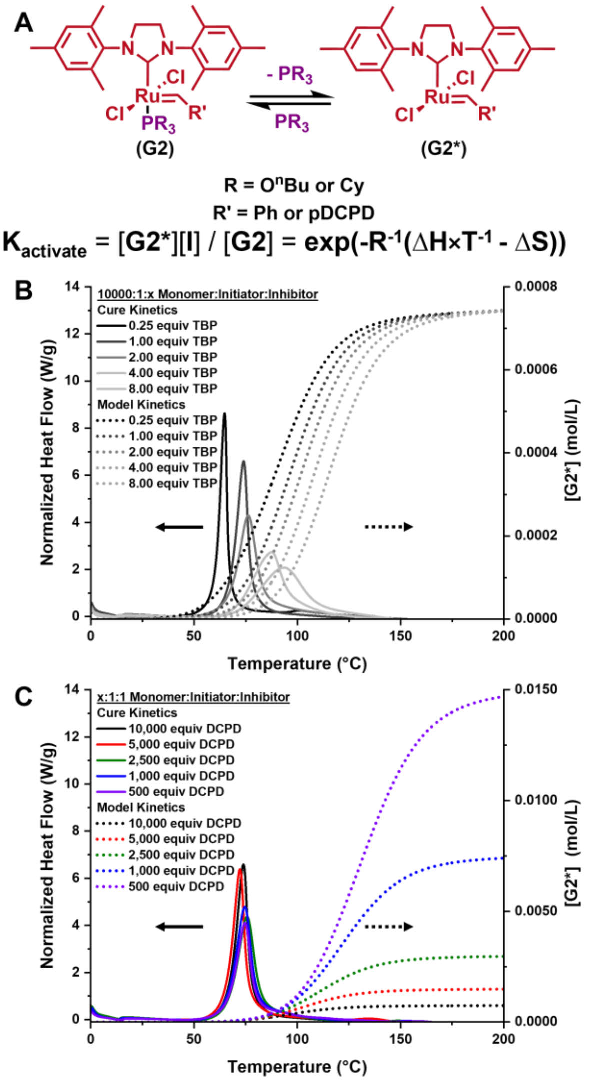

Figure 3: (A) Scheme of inhibition equilibrium with equation relating active initiator with temperature. (B-C) Differential scanning calorimetry (DSC) and [G2*] for varied inhibitor loadings vs temperature at 10,000:1:x and x:1:1 monomer:initiator:inhibitor.

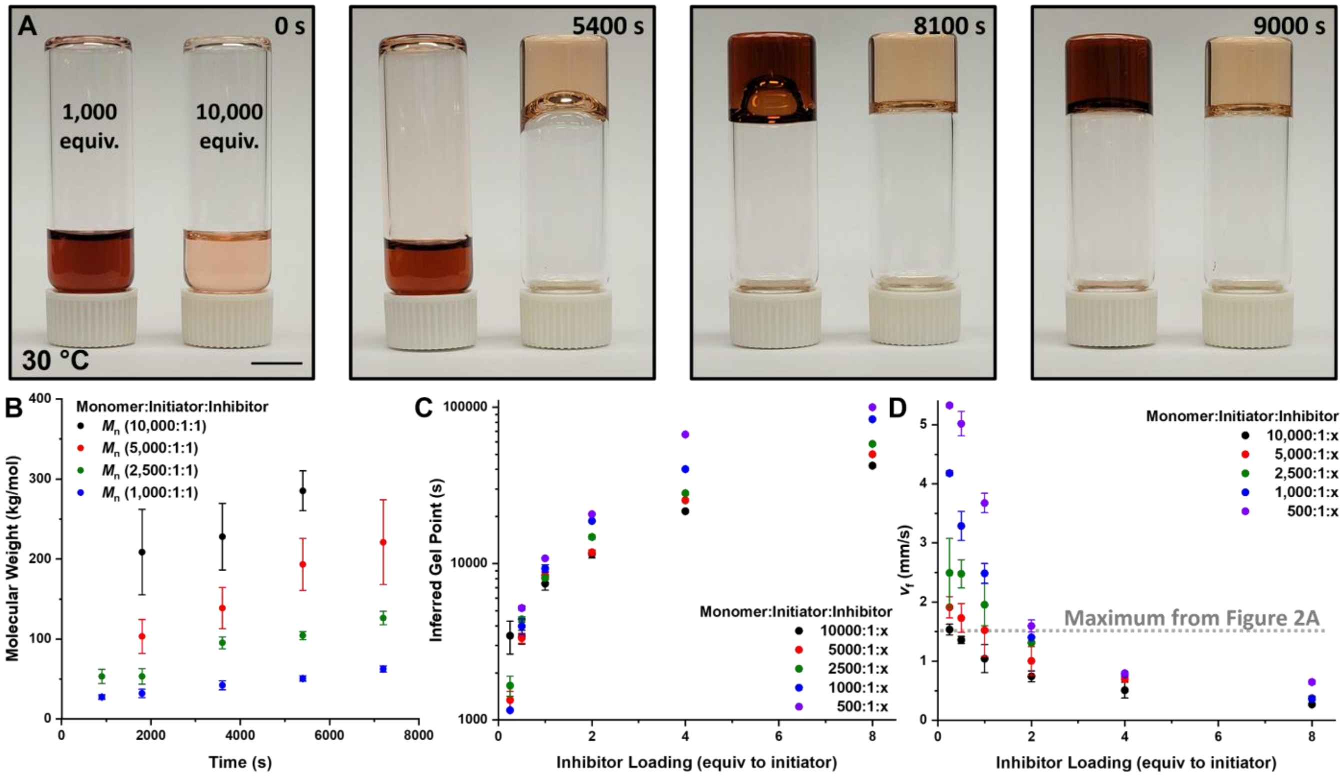

Figure 4: (A) Inverted vial tests for the evaluation of gelation at different t_{rest} for varied monomer loadings showing increased resin pot-life of higher initiator loadings (scale bar=10mm). (B) Molecular weights from ROMP kinetics for x:1:1 at 30 °C before gel point obtained from size exclusion chromatography using conventional calibration from polystyrene standards. (C) Inferred gel point from ROMP inverted vial tests and (D) FROMP front velocity (v_f) for varied loadings of monomer and inhibitor (TBP) to initiator showing rates up to 5.3mm/s.

We systematically explored various monomer-to-initiator loadings, each coupled with inhibitor molar equivalents ranging from 0.25 to 8.00 (10000-500:1:x monomer:initiator:inhibitor), employing both protorheology at 30°C and FROMP kinetics. Protorheology analysis revealed a consistent trend: higher initiator equivalence extended the resin lifetime, delaying the gel point, until reaching the lowest inhibitor loadings (0.25equiv), where the trend reversed (Figure 4C). This inversion stemmed from the inhibitor's diminished ability to effectively deactivate the initiator at such low concentrations. Concurrently, FROMP reaction rates increased as monomer and inhibitor decreased (Figure 4D). The 500:1:0.5 loading achieved a remarkable rate of 5.0±0.2mm/s, while retaining 70% of the resin lifetime. Similarly, the 1,000:1:1 formulation exhibited a rate of 2.5±0.2mm/s and an additional 20% increase in resin lifetime compared to the traditional 10,000:1:1 formulation at 1.0±0.2mm/s, showcasing the significant advancements achieved in optimizing both reaction speed and resin longevity.

FROMP resin formulations that result in higher front velocities without sacrificing pot-life have significant benefits for 3D printing applications. We evaluated the performance of our optimized FROMP resins for direct ink writing (DIW) of several truss structures. We modified the resin rheology through background ROMP, enabling brief shape retention post extrusion from the print nozzle, followed by the precise printing of cantilevers to measure the front velocity (v_f) of the modified resin. A significant increase in v_f (2.70±0.13mm/s) was observed during printing of the modified 1,000:1:1 (monomer:initiator:inhibitor) resin formulation compared with the 10,000:1:1 resin formulation (0.85±0.03mm/s), demonstrating the translation of our strategy to direct ink writing (Figures S74-S81).

To highlight the advantages of the modified resin formulations, we free-form printed prismatic structures consisting of two connected triangles (Figure 5), either offset (±33°) or aligned (0°). The ±33° configuration demonstrated the ability to make prints at an angle without the need for additional support. Remarkably, the ±33° printed parts using the 1,000:1:1 formulation were completed 50s faster than their counterparts using the 10,000:1:1 formulation (Figures 5A-B). We then proceeded to print the 0° parts to assess the integrity of the printed structures (Figure 5C). These 0° printed parts (weighing between 400-500mg) supported a load of 4.6kg (×10,000 mass, Figure 5D) without failing. Impressively, the printed components began to fail only under a 6.8kg load (>×15,000 mass, Figure S82). Coupled with the high thermal stability and energy efficiency, the increased printing rate enhances FROMP based direct in writing as an attractive method for the manufacturing of high-performance thermoset materials.

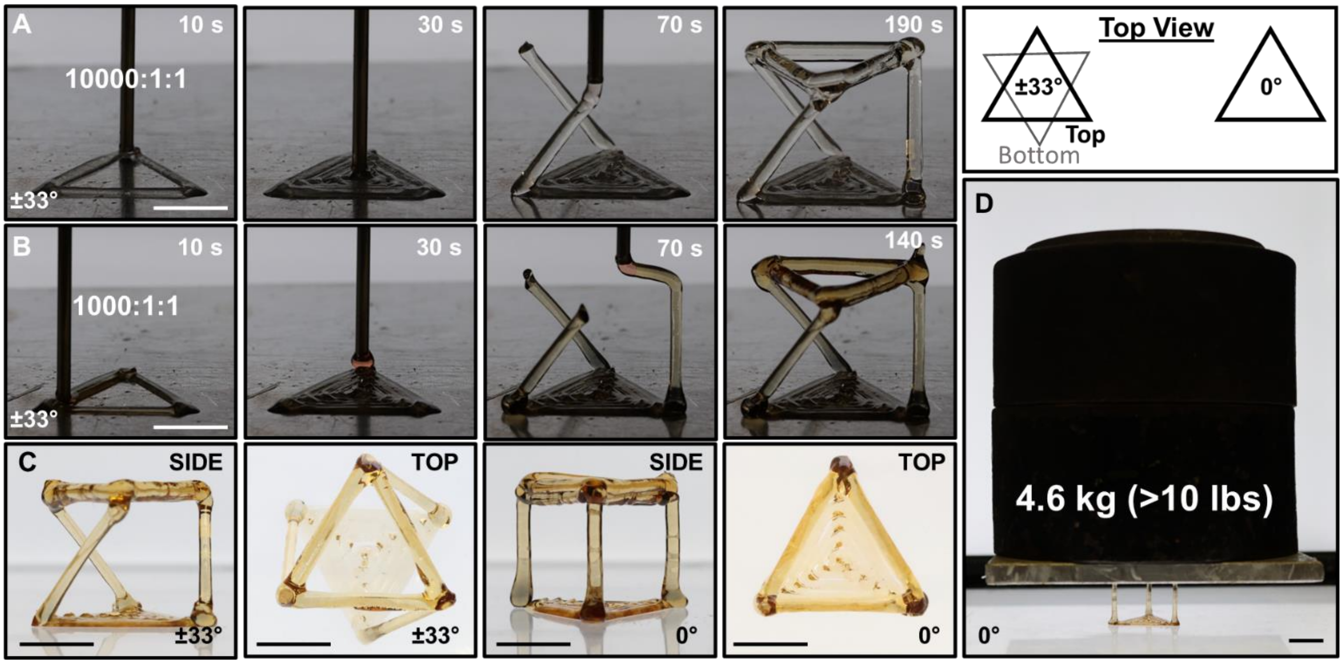

Figure 5: (A) Timelapse for direct ink writing of 10000:1:1 and (B) 1000:1:1 DCPD:G2:TBP on a heated bed for ±33° specimens from FROMP. (C) Images of ±33° and 0° 1000:1:1 post print. (D) 0° printed specimen (~400mg) supporting 4.6kg (scale bars=10mm).

ASSOCIATED CONTENT

Supporting Information

The Supporting Information is available free of charge on the ACS Publications website. PDF describing materials, instrumentation, experimental procedures, inhibitor loadings, modeling, monomer loadings, and direct ink writing.

AUTHOR INFORMATION

Corresponding Author

Jacob J. Lessard - Beckman Institute for Advanced Science and Technology, Department of Chemistry, University of Illinois Urbana–Champaign, Urbana, Illinois 61801, United States;
orcid.org/0000-0003-2962-6472;
email: lessard@illinois.edu

Jeffrey S. Moore - Beckman Institute for Advanced Science and Technology, Department of Chemistry, University of Illinois Urbana–Champaign, Urbana, Illinois 61801, United States;
orcid.org/0000-0001-5841-6269;
email: jsmoore@illinois.edu

Author Contributions

The manuscript was written through contributions of all authors. All authors have given approval to the final version of the manuscript.

Notes

The authors declare no competing financial interests.

ACKNOWLEDGMENT

This work was primarily funded by the Department of Energy (Office of Basic Energy Sciences) as part of the Energy Frontier Research Center titled Regenerative Energy-Efficient Manufacturing of Thermoset Polymeric Materials (REMAT) under award number DE-SC0023457. ZZ would like to acknowledge the NASA's Illinois Space Grant Consortium (ILSGC) Undergraduate Research Opportunity Program (UROP) for sponsoring the summer of 2023. ZSMB would like to acknowledge the Illinois NSF-sponsored Research Experiences for Undergraduates (REU) program for sponsoring the summer of 2023. Additionally, the authors would like to thank Dr. Julian Cooper, Dr. Benjamin Suslick, Dr. Chaimongkol Saengow, Dr. Ignacio Arretche, and Henry M. Wang for their insightful conversations.

REFERENCES

(1.) Ogba, O. M.; Warner, N. C.; O'Leary, D. J.; Grubbs, R. H. Recent advances in ruthenium-based olefin metathesis. *Chem. Soc. Rev.* **2018**, *47*, 4510-4544.
(2) Sutthasupa, S.; Shiotsuki, M.; Sanda, F. Recent advances in ring-opening metathesis polymerization, and application to synthesis of functional materials. *Polym. J.* **2010**, *42*, 905-915.
(3) Grubbs, R. B.; Grubbs, R. H. 50th Anniversary Perspective: Living Polymerization—Emphasizing the Molecule in Macromolecules. *Macromolecules* **2017**, *50*, 6979-6997.
(4) Slugovc, C. The Ring Opening Metathesis Polymerisation Toolbox. *Macromol. Rapid Commun.* **2004**, *25*, 1283-1297.
(5) Leitgeb, A.; Wappel, J.; Slugovc, C. The ROMP toolbox upgraded. *Polymer* **2010**, *51*, 2927-2946.
(6) Gutekunst, W. R.; Hawker, C. J. A General Approach to Sequence-Controlled Polymers Using Macrocyclic Ring Opening Metathesis Polymerization. *J. Am. Chem. Soc.* **2015**, *137*, 8038-8041.
(7) Chen, R.; Benware, S. J.; Cawthern, S. D.; Cole, J. P.; Lessard, J. J.; Crawford-Eng, I. M.; Saxena, R.; Berda, E. B. Assessing structure/property relationships and synthetic protocols in the fabrication of poly(oxanorbornene imide) single-chain nanoparticles. *Eur. Polym. J.* **2019**, *112*, 206-213.
(8) Kobayashi, S.; Pitet, L. M.; Hillmyer, M. A. Regio- and Stereoselective Ring-Opening Metathesis Polymerization of 3-Substituted Cyclooctenes. *J. Am. Chem. Soc.* **2011**, *133*, 5794-5797.

(9) Levi, A. E.; Fu, L.; Lequieu, J.; Horne, J. D.; Blankenship, J.; Mukherjee, S.; Zhang, T.; Fredrickson, G. H.; Gutekunst, W. R.; Bates, C. M. Efficient Synthesis of Asymmetric Miktoarm Star Polymers. *Macromolecules* **2020**, *53*, 702-710.
(10) Self, J. L.; Sample, C. S.; Levi, A. E.; Li, K.; Xie, R.; de Alaniz, J. R.; Bates, C. M. Dynamic Bottlebrush Polymer Networks: Self-Healing in Super-Soft Materials. *J. Am. Chem. Soc.* **2020**, *142*, 7567-7573.
(11) Boydston, A. J.; Xia, Y.; Kornfield, J. A.; Gorodetskaya, I. A.; Grubbs, R. H. Cyclic Ruthenium-Alkylidene Catalysts for Ring-Expansion Metathesis Polymerization. *J. Am. Chem. Soc.* **2008**, *130*, 12775-12782.
(12) Bielawski, C. W.; Benitez, D.; Grubbs, R. H. An "Endless" Route to Cyclic Polymers. *Science* **2002**, *297*, 2041-2044.
(13) Shieh, P.; Nguyen, H. V. T.; Johnson, J. A. Tailored silyl ether monomers enable backbone-degradable polynorbornene-based linear, bottlebrush and star copolymers through ROMP. *Nature Chem.* **2019**, *11*, 1124-1132.
(14) Callmann, C. E.; Thompson, M. P.; Gianneschi, N. C. Poly(peptide): Synthesis, Structure, and Function of Peptide–Polymer Amphiphiles and Protein-like Polymers. *Acc. Chem. Res.* **2020**, *53*, 400-413.
(15) Vaisman, A.; Vidavsky, Y.; Baranov, M.; Lehrer, A.; Baraban, J. H.; Lemcoff, N. G. Latency for All: Enabling Latency of Hoveyda–Grubbs Second-Generation Catalysts by Adding Phosphite Ligands. *J. Am. Chem. Soc.* **2024**, *146*, 73-78.
(16) Jawiczuk, M.; Marczyk, A.; Trzaskowski, B. Decomposition of Ruthenium Olefin Metathesis Catalyst. *Catalysts* **2020**, *10*, 887.
(17) Trnka, T. M.; Morgan, J. P.; Sanford, M. S.; Wilhelm, T. E.; Scholl, M.; Choi, T.-L.; Ding, S.; Day, M. W.; Grubbs, R. H. Synthesis and Activity of Ruthenium Alkylidene Complexes Coordinated with Phosphine and N-Heterocyclic Carbene Ligands. *J. Am. Chem. Soc.* **2003**, *125*, 2546-2558.
(18) Hong, S. H.; Day, M. W.; Grubbs, R. H. Decomposition of a Key Intermediate in Ruthenium-Catalyzed Olefin Metathesis Reactions. *J. Am. Chem. Soc.* **2004**, *126*, 7414-7415.
(19) Bailey, G. A.; Foscato, M.; Higman, C. S.; Day, C. S.; Jensen, V. R.; Fogg, D. E. Bimolecular Coupling as a Vector for Decomposition of Fast-Initiating Olefin Metathesis Catalysts. *J. Am. Chem. Soc.* **2018**, *140*, 6931-6944.
(20) Neary, W. J.; Kennemur, J. G. Variable Temperature ROMP: Leveraging Low Ring Strain Thermodynamics To Achieve Well-Defined Polypentenamers. *Macromolecules* **2017**, *50*, 4935-4941.
(21) Courchay, F. C.; Sworen, J. C.; Ghiviriga, I.; Abboud, K. A.; Wagener, K. B. Understanding Structural Isomerization during Ruthenium-Catalyzed Olefin Metathesis: A Deuterium Labeling Study. *Organometallics* **2006**, *25*, 6074-6086.
(22) Suslick, B. A.; Hemmer, J.; Groce, B. R.; Stawiasz, K. J.; Geubelle, P. H.; Malucelli, G.; Mariani, A.; Moore, J. S.; Pojman, J. A.; Sottos, N. R. Frontal Polymerizations: From Chemical Perspectives to Macroscopic Properties and Applications. *Chem. Rev.* **2023**, *123*, 3237-3298.
(23) Pojman, J. A. 4.38 - Frontal Polymerization. In *Polymer Science: A Comprehensive Reference*, Matyjaszewski, K., Möller, M. Eds.; Elsevier, 2012; pp 957-980.
(24) Li, Q.; Shen, H.-X.; Liu, C.; Wang, C.-F.; Zhu, L.; Chen, S. Advances in frontal polymerization strategy: From fundamentals to applications. *Prog. Polym. Sci.* **2022**, *127*, 101514.
(25) Stawiasz, K. J.; Wendell, C. I.; Suslick, B. A.; Moore, J. S. Photoredox-Initiated Frontal Ring-Opening Metathesis Polymerization. *ACS Macro Lett.* **2022**, 780-784.
(26) Lessard, J. J.; Kaur, P.; Paul, J. E.; Chang, K. M.; Sottos, N. R.; Moore, J. S. Switching Frontal Polymerization Mechanisms: FROMP and FRaP. *ACS Macro Lett.* **2022**, *11*, 1097-1101.
(27) Stawiasz, K. J.; Paul, J. E.; Schwarz, K. J.; Sottos, N. R.; Moore, J. S. Photoexcitation of Grubbs' Second-Generation Catalyst Initiates Frontal Ring-Opening Metathesis Polymerization. *ACS Macro Lett.* **2020**, *9*, 1563-1568.
(28) Lloyd, E. M.; Feinberg, E. C.; Gao, Y.; Peterson, S. R.; Soman, B.; Hemmer, J.; Dean, L. M.; Wu, Q.; Geubelle, P. H.; Sottos, N. R.; Moore, J. S. Spontaneous Patterning during Frontal Polymerization. *ACS Cent. Sci.* **2021**, *7*, 603-612.
(29) Goli, E.; Robertson, I. D.; Geubelle, P. H.; Moore, J. S. Frontal Polymerization of Dicyclopentadiene: A Numerical Study. *J. Phys. Chem. B* **2018**, *122*, 4583-4591.
(30) Robertson, I. D.; Pruitt, E. L.; Moore, J. S. Frontal Ring-Opening Metathesis Polymerization of Exo-Dicyclopentadiene for Low Catalyst Loadings. *ACS Macro Lett.* **2016**, *5*, 593-596.
(31) Ruiu, A.; Sanna, D.; Alzari, V.; Nuvoli, D.; Mariani, A. Advances in the frontal ring opening metathesis polymerization of dicyclopentadiene. *J. Polym. Sci. A Polym. Chem.* **2014**, *52*, 2776-2780.
(32) Mariani, A.; Fiori, S.; Chekanov, Y.; Pojman, J. A. Frontal Ring-Opening Metathesis Polymerization of Dicyclopentadiene. *Macromolecules* **2001**, *34*, 6539-6541.
; Lessard, J. J.; Paul, J. E.; Sottos, N. R.; Moore, J. S. Rapid Controlled Synthesis of Large Polymers by Frontal Ring-Opening Metathesis Polymerization. *Macromolecules* **2023**, *56*, 1527-1533.
(34) Suslick, B. A.; Stawiasz, K. J.; Paul, J. E.; Sottos, N. R.; Moore, J. S. Survey of Catalysts for Frontal Ring-Opening Metathesis Polymerization. *Macromolecules* **2021**, *54*, 5117-5123.
(35) Davydovich, O.; Paul, J. E.; Feist, J. D.; Aw, J. E.; Balta Bonner, F. J.; Lessard, J. J.; Tawfick, S.; Xia, Y.; Sottos, N. R.; Moore, J. S. Frontal Polymerization of Dihydrofuran Comonomer Facilitates Thermoset Deconstruction. *Chem. Mater.* **2022**, *34*, 8790-8797.
(36) Dean, L. M.; Wu, Q.; Alshangiti, O.; Moore, J. S.; Sottos, N. R Rapid Synthesis of Elastomers and Thermosets with Tunable Thermomechanical Properties. *ACS Macro Lett.* **2020**, *9*, 819-824.
(37) Wang, H. M.; Suslick, B. A.; Lessard, J. J.; Yu, C. H.; Saengow, C.; Ewoldt, R. H.; Moore, J. S. Frontal Polymerization of Stereoisomers: Distinct Microstructures and Properties in Endo- and Exo-Dicyclopentadiene Thermosets. *Macromolecules* **2024**, *57*, 142-149.
(38) Robertson, I. D.; Yourdkhani, M.; Centellas, P. J.; Aw, J. E.; Ivanoff, D. G.; Goli, E.; Lloyd, E. M.; Dean, L. M.; Sottos, N. R.; Geubelle, P. H.; et al. Rapid energy-efficient manufacturing of polymers and composites via frontal polymerization. *Nature* **2018**, *557*, 223-227.
(39) Robertson, I. D.; Dean, L. M.; Rudebusch, G. E.; Sottos, N. R.; White, S. R.; Moore, J. S. Alkyl Phosphite Inhibitors for Frontal Ring-Opening Metathesis Polymerization Greatly Increase Pot Life. *ACS Macro Lett.* **2017**, *6*, 609-612.
(40) Bielawski, C. W.; Grubbs, R. H. Living ring-opening metathesis polymerization. *Prog. Polym. Sci.* **2007**, *32*, 1-29.
(41) Garg, M.; Aw, J. E.; Zhang, X.; Centellas, P. J.; Dean, L. M.; Lloyd, E. M.; Robertson, I. D.; Liu, Y.; Yourdkhani, M.; Moore, J. S.; et al. Rapid synchronized fabrication of vascularized thermosets and composites. *Nature Commun.* **2021**, *12*, 2836.
(42) Aw, J. E.; Zhang, X.; Nelson, A. Z.; Dean, L. M.; Yourdkhani, M.; Ewoldt, R. H.; Geubelle, P. H.; Sottos, N. R. Self-Regulative Direct Ink Writing of Frontally Polymerizing Thermoset Polymers. *Adv. Mater. Technol.* **2022**, *7*, 2200230.

(43) Chang, K. M.; Das, D.; Salvati Iii, L.; Dean, L. M.; Keshari, R.; Garg, M.; Dlott, D. D.; Chasiotis, I.; Sottos, N. R. Durable and impact-resistant thermoset polymers for the extreme environment of low Earth orbit. *Extreme Mech. Lett.* **2023**, *64*, 102089.
(44) Suslick, B. A.; Alzate-Sanchez, D. M.; Moore, J. S. Scalable Frontal Oligomerization: Insights from Advanced Mass Analysis. *Macromolecules* **2022**, *55*, 8234-8241.
(45) Lloyd, E. M.; Cooper, J. C.; Shieh, P.; Ivanoff, D. G.; Parikh, N. A.; Mejia, E. B.; Husted, K. E. L.; Costa, L. C.; Sottos, N. R.; Johnson, J. A.; Moore, J. S. Efficient Manufacture, Deconstruction, and Upcycling of High-Performance Thermosets and Composites. *ACS Applied Engineering Materials* **2023**, *1*, 477-485.
(46) M. T. Hossain, R. H. E. Protorheology. *J. Rheol.* **2024**, *68, 113–144.*
(47) Wool, R. P. Polymer Entanglements. *Macromolecules* **1993**, *26*, 1564-1569.

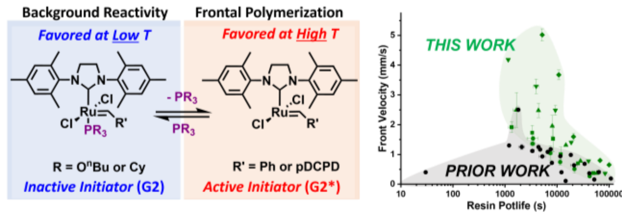

Background Reactivity
Favored at Low T
Frontal Polymerization
Favored at High T
- PR3
PR3
R = OnBu or Cy
Inactive Initiator (G2)
R' = Ph or pDCPD
Active Initiator (G2*)
THIS WORK
PRIOR WORK
Front Velocity (mm/s)
Resin Potlife (s)